

Differentially Private Boxplots

Kelly Ramsay and Jairo Diaz-Rodriguez

Department of Mathematics and Statistics
York University
Toronto, Ontario M3J 1P3

October 21, 2024

Abstract

Despite the potential of differentially private data visualization to harmonize data analysis and privacy, research in this area remains relatively underdeveloped. Boxplots are a widely popular visualization used for summarizing a dataset and for comparison of multiple datasets. Consequently, we introduce a differentially private boxplot. We evaluate its effectiveness for displaying location, scale, skewness and tails of a given empirical distribution. In our theoretical exposition, we show that the location and scale of the boxplot are estimated with optimal sample complexity, and the skewness and tails are estimated consistently. In simulations, we show that this boxplot performs similarly to a non-private boxplot, and it outperforms a boxplot naively constructed from existing differentially private quantile algorithms. Additionally, we conduct a real data analysis of Airbnb listings, which shows that comparable analysis can be achieved through differentially private boxplot visualization.

1 Introduction

It is now well established that differential privacy (Dwork et al., 2006) is a powerful framework for protecting the privacy of individuals' data. As a result, a plethora of differentially private data analysis tools have been developed over the last several decades (Dwork, 2008; Ji et al., 2014; Liu et al., 2023). However, one area that has been considerably underdeveloped is that of differentially private visualization. This is despite the fact that data visualization is a key tool in exploratory analysis, which is an essential component of data analysis. In fact, in a recent study of data analysts and practitioners, Garrido et al. (2023) found that “most analysts employed aggregations and visualizations to fulfill their use case,” rather than machine learning models.

Differentially private versions of several popular visualizations have been considered in the literature. There has been substantial study of the differentially private histogram (Hay et al., 2010; Li et al., 2010; Acs et al., 2012; Kellaris

and Papadopoulos, 2013; Xu et al., 2013; Zhang et al., 2014; Budiu et al., 2022). Visualizations based on clustering (Hongde et al., 2014), for mobility data (He et al., 2016), heatmaps (Zhang et al., 2016) and scatterplots (Panavas et al., 2024) have also been considered.

Surprisingly, despite its widespread use, a differentially private boxplot has not been directly studied. Boxplots, invented by Tukey et al. (1977), are used for visualizing the characteristics of a univariate sample, as well as for visualizing the relationship between a continuous variable and a categorical variable. Despite its simplicity, many key distributional characteristics can be evaluated from the boxplot: namely, location, scale, skewness, and tails. This has made it popular among practitioners.

In addition, its simplicity is beneficial from a privacy standpoint. The boxplot only requires estimating a few summary statistics in order to convey the distributional characteristics of a univariate sample, making the boxplot efficient in its use of privacy budget. For instance, by contrast, a histogram can also be used to convey the same information. However, a histogram is generally a consistent estimate of the population density, which intuitively, should then require more noise to ensure privacy.

Motivated by these observations, we develop and study a differentially private boxplot. Our contributions are as follows: We introduce a differentially private boxplot and evaluate its ability to convey location, scale, skewness and tails both theoretically and empirically. We show that the inner quantiles used for the location and scale of the boxplot are estimated optimally (Theorem 1). We then show that tails and skewness are estimated consistently (Theorem 4). Through extensive simulations, we show that the proposed boxplot is often more accurate than one naively constructed via popular, existing differentially private quantile methods (see Section 5). We also conduct a differentially private exploratory data analysis, demonstrating the utility of the proposed boxplots, as well as their limitations (see Section 6). As a by-product of our work, we develop some new results concerning private quantiles. We introduce a minimax lower bound on private quantile estimation, and show that when the number of quantiles is small, the quantile algorithms `JointExp` (Gillenwater et al., 2021) and `PrivateQuantile` (Smith, 2011) attain this lower bound, up to logarithmic factors. We also theoretically confirm the empirical observation of Durfee (2023), which says that the `unbounded` quantile algorithm performs better than existing algorithms for estimating extreme quantiles. We show that `JointExp` is inconsistent for extreme quantiles (Lemma 8), where the `unbounded` algorithm of Durfee (2023) is consistent (Lemma 7). We also present simulations comparing four differentially private quantile algorithms, those of Smith (2011); Gillenwater et al. (2021); Kaplan et al. (2022) and Durfee (2023).

Before turning to our main results, we mention some other related works. Nanayakkara et al. (2022) developed a plot to visualize privacy utility trade-offs. Zhou et al. (2022) developed `DPVisCreator`, a visualization system, which relies on publishing a synthetic dataset. Visualizations in other privacy models were considered by Dasgupta and Kosara (2011); Dasgupta et al. (2013, 2019), and recently reviewed by Bhattacharjee et al. (2020). In addition, a related area

is that of differentially private quantile estimation (Smith, 2011; Gillenwater et al., 2021; Kaplan et al., 2022; Alabi et al., 2022; Durfee, 2023; Lalanne et al., 2023a,b). One could apply any one of these algorithms to create a differentially private boxplot. We show in Section 5 that this approach is often less accurate than the proposed methodology.

2 Preliminaries

First, we briefly review the boxplot. It is also helpful to introduce some notation used throughout the paper. We define a dataset of size $n \in \mathbb{N}$ to be a set of n real numbers. Let \mathcal{D}_n be the set of datasets of size n and let $\mathbf{X}_n = \{X_1, \dots, X_n\}$ be a dataset size n . In this work, we assume the analyst has access to a dataset, denoted by \mathbf{X}_n . The non-private boxplot constructed from the data is taken to be the boxplot computed on the empirical measure of the dataset \mathbf{X}_n , denoted by $\hat{\nu}$.

The boxplot consists of a box with a line drawn through it, with two whiskers emanating from the lower and upper bounds of the box. Specific points are sometimes indicated above or below the whiskers. The central line inside the box marks the median of the dataset. The box itself is constructed from the quartiles, detailing the middle 50% of \mathbf{X}_n . The lower (upper) whisker is constructed from the larger (smaller) of the minimum (maximum) of \mathbf{X}_n and the lower (upper) quartile of \mathbf{X}_n minus (plus) 1.5 times the interquartile range of \mathbf{X}_n . Lastly, any points in \mathbf{X}_n falling outside of the whiskers are added to the plot. See Figure 2 for an example. The boxplot describes various characteristics of \mathbf{X}_n . The median line approximates the *location* of \mathbf{X}_n . The box itself approximates the spread or *scale* of \mathbf{X}_n . The *skewness* of \mathbf{X}_n can be approximated as follows: A median line placed in the center of the box, along with whiskers that are similar in magnitude, suggests a symmetric distribution. A median line placed away from the center of the box or asymmetric whiskers indicates skewness. Additionally, the *tails* can be assessed by the number of points beyond the whiskers. Many such points signify outliers or heavy tails, highlighting data points that deviate significantly from the rest.

Next, we introduce differential privacy. First, we say that $\mathbf{Y}_n \in \mathcal{D}_n$, is adjacent to \mathbf{X}_n if \mathbf{X}_n and \mathbf{Y}_n differ in exactly one point. Let \mathcal{A}_n be the set of pairs of adjacent datasets of size n . Next, denote by $P_{\mathbf{X}_n}$ a probability measure which depends on \mathbf{X}_n . For a space S , let $\mathcal{B}(S)$ denote the Borel sets of S and let $\mathcal{M}_1(S)$ be the set of Borel probability measures over S . Formally, $P_{\mathbf{X}_n}$ is a map from \mathbb{R}^n to $\mathcal{M}_1(\mathbb{R}^d)$, for some $d \in \mathbb{N}$. We can now define differential privacy.

Definition 1. The quantity $\theta \sim P_{\mathbf{X}_n}$ is ϵ -differentially private if

$$\sup_{(\mathbf{X}_n, \mathbf{Y}_n) \in \mathcal{A}_n} \sup_{B \in \mathcal{B}(\mathbb{R}^d)} \frac{P_{\mathbf{X}_n}(B)}{P_{\mathbf{Y}_n}(B)} \leq e^\epsilon. \quad (1)$$

Here, θ is a d -dimensional differentially private quantity and ϵ is the privacy budget, where values of ϵ which are closer to zero enforce stricter privacy constraints.

The proposed differentially private boxplot makes use of existing differentially private algorithms. Specifically, the Laplace mechanism, and algorithms for computing differentially private quantiles. The Laplace mechanism (Dwork et al., 2006) is a fundamental mechanism for constructing differentially private statistics. Let Z be a standard Laplace random variable. Specifically, for a statistic $T: \mathcal{D}_n \rightarrow \mathbb{R}$, define its global sensitivity to be $\sup_{(\mathbf{X}_n, \mathbf{Y}_n) \in \mathcal{A}_n} |T(\mathbf{X}_n) - T(\mathbf{Y}_n)|$. If T has global sensitivity bounded by 1, then $\tilde{T} = T(\mathbf{X}_n) + Z/\epsilon$ is a differentially private quantity. This is known as the Laplace mechanism.

Of course, a private boxplot relies on differentially private quantiles. The proposed private boxplot relies on the **unbounded** algorithm of Durfee (2023) and the **JointExp** algorithm of Gillenwater et al. (2021). These algorithms are the main focus of our theoretical exposition. We do, however, consider the performance of the naive boxplot constructed via the algorithms of Smith (2011), Kaplan et al. (2022) and Durfee (2023) in our simulation study, see Section 5. We also discuss the extent to which our theoretical results extend to these other algorithms, see Remark 3.

We now give a brief overview of **JointExp** and **unbounded**. **JointExp** works as follows: Suppose we wish to estimate $m \in \mathbb{N}$ quantiles of levels $0 < q_1 < \dots < q_m < 1$. For an integer $k \in \mathbb{N}$, let $[k]$ denote the set $\{1, \dots, k\}$. Define the j th quantile generated by **JointExp** for a given $j \in [m]$ to be $\tilde{\xi}_{q_j}$, and let $\tilde{\xi}_q = (\tilde{\xi}_{q_1}, \dots, \tilde{\xi}_{q_m})$. For a given $\nu \in \mathcal{M}_1(\mathbb{R})$, let F_ν be the cumulative distribution function of ν and, if it exists, let f_ν be its probability density function. Now, define the following utility function: $\phi(x) = -\sum_{j=1}^{m+1} |F_\nu(x_j) - F_\nu(x_{j-1}) - (q_j - q_{j-1})|$, where $x_0 = -\infty < x_1 < \dots < x_m < x_{m+1} = \infty$, $q_0 = 0$ and $q_{m+1} = 1$. Then $\tilde{\xi}_q$ has law $Q_{\mathbf{X}_n}$, where $f_{Q_{\mathbf{X}_n}} \propto \exp(-n\phi(x)/2\epsilon)\mathbb{1}\{x \in [a, b]\}$. It was shown by Gillenwater et al. (2021) that $\tilde{\xi}_q$ is ϵ -differentially private. Furthermore, Lalanne et al. (2023b) showed that this algorithm is consistent for continuous distributions. If one suspects that the population distribution contains atoms, then we recommend that one uses the jittering modification proposed by Lalanne et al. (2023b). We show in Section 4 that, for a large class of distributions, this algorithm has optimal sample complexity for estimating a single quantile, and therefore, for the scale and location of the boxplot. (Here we are only interested in estimating three quantiles, and so, how sample complexity scales in m is not of particular concern.)

The **unbounded** algorithm produces a private quantile given a lower bound on the data. We present a slightly modified version, which performs better for extreme quantiles. For a given quantile $q \in [1/2, 1]$ and $a > 0$, let V_0, V_1, \dots be independent, standard exponential random variables and let $\beta_n > 1$. Define $i^* = \inf\{i \in \mathbb{N}: F_\nu(\beta_n^i - a - 1) + \frac{2}{n\epsilon}V_i \geq q + V_0 \frac{2}{n\epsilon}\}$. The quantile estimate generated by the **unbounded** algorithm is given by: $\tilde{\psi}_q = \beta_n^{i^*} - a - 1$. If $q \in (0, 1/2)$, then, we apply the above procedure to the dataset $-\mathbf{X}_n = \{-X_1, \dots, -X_n\}$, with input parameters $1 - q + 1/n$ and $a = -b$. It follows from (Durfee, 2023) that this algorithm is ϵ -differentially private. In the proposed differentially private boxplot algorithm, we use **unbounded** to estimate the minimum and maximum of the dataset. For a measure $\nu \in \mathcal{M}_1(\mathbb{R})$, let $\xi_{p,\nu} = \inf\{x \in \mathbb{R}: p \leq F_\nu(x)\}$

be the associated p th quantile, $\min(\nu) = \inf\{x: F_\nu(x) > 0\}$ and $\max(\nu) = \inf\{x: F_\nu(x) = 1\}$. We show that if \mathbf{X}_n is an independent sample from ν , then $\tilde{\psi}_1$ is weakly consistent for $\max(\nu)$, and $\tilde{\psi}_{1/n}$ is weakly consistent for $\min(\nu)$, see Lemma 7. By contrast, we show that **JointExp** is inconsistent for $\min(\nu)$ when $q = 1/n$, unless $a = \min(\nu)$, see Lemma 8. Lastly, we note that instead of exponential noise, one could also use Laplace or Gumbel noise (Durfee, 2023). We found this to make little difference in simulation, and so we only present the version which incorporates exponential noise.

3 A differentially private boxplot

We can now introduce the differentially private boxplot. Let $q = (1/4, 1/2, 3/4)$ and $\text{IQR} = \tilde{\xi}_{3/4} - \tilde{\xi}_{1/4}$. Given lower and upper bounds on the data a and b ¹, we first generate the minimum and maximum estimates using the **unbounded** algorithm, $\tilde{\psi}_{1/n}$ and $\tilde{\psi}_1$. Critically, we use the unbounded algorithm because **JointExp** (and, by consequence, **PrivateQuantile** and **ApproxQuantile**) are inconsistent for estimating the aforementioned extreme quantiles, unless the input bounds a and b match $\min(\nu)$ and $\max(\nu)$, respectively, see Lemma 8. Next, we run **JointExp** to generate $\tilde{\xi}_q$. The box bounds and center line are then constructed from $(\tilde{\xi}_{1/4}, \tilde{\xi}_{1/2}, \tilde{\xi}_{3/4})$. Letting $\tilde{\ell}_1 = \tilde{\xi}_{1/4} - \text{IQR}$, $\tilde{u}_1 = \tilde{\xi}_{3/4} + \text{IQR}$ and λ_n be a sequence decreasing to 0, the lower and upper whisker are defined as

$$\tilde{\ell} = \begin{cases} \tilde{\ell}_1 & \tilde{\xi}_{1/n} \leq \lambda_n |\tilde{\ell}_1| + \tilde{\ell}_1 \\ \tilde{\psi}_{1/n} & \tilde{\xi}_{1/n} > \lambda_n |\tilde{\ell}_1| + \tilde{\ell}_1 \end{cases}$$

$$\tilde{u} = \begin{cases} \tilde{u}_1 & \tilde{\xi}_1 \geq \tilde{u}_1 - \lambda_n |\tilde{u}_1| \\ \tilde{\psi}_1 & \tilde{\xi}_1 < \tilde{u}_1 - \lambda_n |\tilde{u}_1| \end{cases},$$

respectively. To elaborate, the role of the minimum and the maximum of the dataset in a traditional boxplot is played by the estimated extreme quantiles $\tilde{\psi}_{1/n}$ and $\tilde{\psi}_1$. Given that estimated extreme quantiles are more variable than the estimated inner quantiles, we set a given whisker equal to its associated extreme quantile only when that quantile is at least $(\lambda_n \times 100)\%$ shorter than the quantity based on the noisy interquartile range. We take $\lambda_n = n^{-1/4}$. Several other values of λ_n were tested in simulation, see Appendix B.2.

A traditional boxplot also plots the observations which lie above and below the upper and lower whiskers, respectively. We cannot release such data points under the constraints of differential privacy. Instead, we plot a noisy version of the number of points above \tilde{u} , denoted \tilde{o}_u and below $\tilde{\ell}$, denoted \tilde{o}_ℓ . These are generated via the Laplace mechanism, where it is easy to see that the count

¹If one does not wish to supply input bounds for the data, one can use the “fully unbounded” version of **unbounded** (Durfee, 2023). However, in simulation, (see Section 5), we have observed that the procedure is still accurate, even when the input bounds are very loose.

of observations above or below a threshold has global sensitivity 1. Lastly, we attribute less privacy budget for computing the outliers, as we deem these values to be of less interest than the box itself. We assign each noisy outlyingness number a privacy budget of $\epsilon/16$. Together, these seven values make up the differentially private boxplot. See Figure 3 for an example of the proposed private boxplot. The algorithm, which we call `DPBoxplot`, is summarized in Algorithm 1. Note that the time and space complexities of `DPBoxplot` are given by the maximum of those of the differentially private quantile algorithms `unbounded` and `JointExp` (Gillenwater et al., 2021; Durfee, 2023). For example, an `unbounded` quantile can be generated in linear time. In addition, it follows directly by sequential composition that `DPBoxplot` is ϵ -differentially private.

Algorithm 1: `DPBoxplot`

```

input:  $\mathbf{X}_n, \epsilon, a, b, \lambda_n$ 
// Construct the private quantiles2
 $\tilde{\psi}_1 \leftarrow \text{unbounded}(1, a, b, 3\epsilon/16)$ ;
 $\tilde{\psi}_{1/n} \leftarrow \text{unbounded}(1/n, a, b, 3\epsilon/16)$ ;
 $\tilde{\xi}_q \leftarrow \text{JointExp}(q, a, b, \epsilon/2)$ ;
// Ensure the box contains the median
 $\tilde{\xi}_{1/4} \leftarrow \tilde{\xi}_{1/4} \wedge \tilde{\xi}_{1/2}$ ;
 $\tilde{\xi}_{3/4} \leftarrow \tilde{\xi}_{3/4} \vee \tilde{\xi}_{1/2}$ ;
// Construct the whiskers and outlyingness counts
 $\tilde{\ell} \leftarrow \tilde{\xi}_{1/4} - 1.5(\tilde{\xi}_{3/4} - \tilde{\xi}_{1/4})$ ;
 $\tilde{u} \leftarrow \tilde{\xi}_{3/4} + 1.5(\tilde{\xi}_{3/4} - \tilde{\xi}_{1/4})$ ;
if  $|\tilde{\psi}_{1/n}| > \lambda_n |\tilde{\ell}| + \tilde{\ell}$  then
    |  $\tilde{\ell} \leftarrow \tilde{\psi}_{1/n}$ ;
    |  $\tilde{o}_\ell \leftarrow 0$ ;
else
    |  $\tilde{o}_\ell \leftarrow \sum_{i=1}^n \mathbb{1}\{x_i < \tilde{\ell}\} + \text{Laplace}(0, \frac{1}{\epsilon/16})$ ;
end
if  $|\tilde{\psi}_1| < \tilde{u} - \lambda_n |\tilde{u}|$  then
    |  $\tilde{u} \leftarrow \tilde{\psi}_1$ ;
    |  $\tilde{o}_u \leftarrow 0$ ;
else
    |  $\tilde{o}_u \leftarrow \sum_{i=1}^n \mathbb{1}\{x_i > \tilde{u}\} + \text{Laplace}(0, \frac{1}{\epsilon/16})$ ;
end
return  $\tilde{B}(\mathbf{X}_n, \epsilon) = (\tilde{o}_\ell, \tilde{\ell}, \tilde{\xi}_{1/4}, \tilde{\xi}_{1/2}, \tilde{\xi}_{3/4}, \tilde{u}, \tilde{o}_u)$ 

```

²In Algorithm 1, for $a, b \in \mathbb{R}$, $a \vee b$ ($a \wedge b$) denotes the maximum (minimum) of a and b .

4 Theoretical results

In this section, we derive several results concerning the different elements of the private boxplot. We now assume that the dataset \mathbf{X}_n consists of n independent, identically distributed random variables drawn from a population measure $\nu \in \mathcal{M}_1(\mathbb{R})$. We first prove an upper bound on the sample complexity of the inner quantiles generated from `JointExp`. We then prove a minimax lower bound for privately estimating a quantile from a population measure lying in a general set, which matches the upper bound up to logarithmic terms. We then prove that the whiskers and outlyingness numbers are weakly consistent for their population counterparts.

We now define a boxplot rigorously, as a function of a measure on the set of real numbers, which is convenient mathematically. The non-private boxplot constructed from the data is taken to be the boxplot computed on the empirical measure of the dataset \mathbf{X}_n , denoted by $\hat{\nu}$. For a measure $\nu \in \mathcal{M}_1(\mathbb{R})$, let $\text{IQR}(\nu) = \xi_{3/4,\nu} - \xi_{1/4,\nu}$. Now, letting $\ell_{1,\nu} = \xi_{1/4,\nu} - \text{IQR}(\nu)$ and $u_{1,\nu} = \xi_{3/4,\nu} + \text{IQR}(\nu)$, the whiskers are defined as $\ell_\nu = \ell_{1,\nu} \vee \min(\nu)$ and $u_\nu = u_{1,\nu} \wedge \max(\nu)$. Lastly, we can define $o_{\ell,\nu} = F_\nu(\ell_\nu) - \nu(\{X = \ell_\nu\})$, $o_{u,\nu} = 1 - F_\nu(u_\nu)$. The ‘population’ boxplot is the following seven number summary $B(\nu) = (o_{\ell,\nu}, \ell_\nu, \xi_{1/4,\nu}, \xi_{1/2,\nu}, \xi_{3/4,\nu}, u_\nu, o_{u,\nu})$. Similarly, we can define the differentially private boxplot $\tilde{B}(\mathbf{X}_n, \epsilon) = \tilde{B}(\hat{\nu}, \epsilon) = (\tilde{o}_\ell, \tilde{\ell}, \tilde{\xi}_{1/4}, \tilde{\xi}_{1/2}, \tilde{\xi}_{3/4}, \tilde{u}, \tilde{o}_u)$.

For $L, r > 0$ and $q \in (0, 1)$, let $\mathcal{G}_{L,r,q}$ be the set of absolutely continuous measures $\nu \in \mathcal{M}_1(\mathbb{R})$ such that $\inf_{\xi_q - r \leq x \leq \xi_q + r} f_\nu(x) \geq L > 0$. Our first result gives an upper bound on the sample complexity of the private quantiles generated via `JointExp`. For $0 < q_1 < \dots < q_m < 1$ and $\nu \in \mathcal{M}_1(\mathbb{R})$, let $q = (q_1, \dots, q_m)$ and define $\xi_{q,\nu} = (\xi_{q_1,\nu}, \dots, \xi_{q_m,\nu})$.

Theorem 1. *For $-\infty < a < b < \infty$ and $q = (q_1, \dots, q_m)$ so that $0 < q_1 < \dots < q_m < 1$, if $\nu \in \cap_{i=1}^m \mathcal{G}_{L,r,q_i}$ is such that $\sup_{x \in [a,b]} f_\nu(x) \leq K < \infty$ and $a \leq \xi_{q_1,\nu} \leq \dots \leq \xi_{q_m,\nu} \leq b$, then there exists a universal constant $C > 0$ such that for all $0 < \gamma < 1$ and $t \leq r$, it holds that $\|\xi_{q,\hat{\nu}} - \xi_{q,\nu}\| \leq t$ with probability $1 - \gamma$, provided that*

$$n \geq C \left(m^{5/2} \frac{\log(1/\gamma) \vee m \log(m/ctL)}{t^2 L^2} \vee m^2 \frac{\log(1/\gamma) \vee \log\left(\frac{K(b-a)}{q_1 \wedge (1-q_m) \wedge tL}\right)}{tL\epsilon} \right).$$

The proof of Theorem 1 relies on a general bound for the exponential mechanism detailed by Ramsay et al. (2024), and so we defer it to Appendix A. Note that the upper bound given in Theorem 1 has suboptimal scaling in m , the `ApproxQuantile` algorithm of Kaplan et al. (2022) obtains logarithmic scaling in m . However, in this context, $m = 3$, and we are not so concerned about this fact.

Next, we present a minimax lower bound for estimating a single quantile subject to differential privacy, which in turn implies a lower bound for estimating m quantiles. Again, since our main interest is in boxplot estimation, we are not concerned about optimal scaling in m . Next, for a set S , let $\tilde{\mathcal{M}}_{1,\epsilon,n}(S)$ be the set of maps from $\hat{\nu}$ to $\mathcal{M}_1(S)$ which satisfy (1). Note $\tilde{\mathcal{M}}_{1,\epsilon,n}(S)$ is just a formal way of writing the set of all differentially private estimators which lie in S . Let $h_q(x) = x\sqrt{(-\log x - [\Phi^{-1}(q)]^2/2)/\pi}$, $C_q = \operatorname{argmax}_{x>0} h_q(x)$ and denote the minimax risk for differentially private quantile estimation by $\mathcal{R}(\epsilon, L, r, q) = \inf_{T_\epsilon \sim \tilde{\mathcal{M}}_{1,\epsilon,n}(\mathbb{R})} \sup_{\nu \in \mathcal{G}_{L,r,q}} \mathbb{E}|T_\epsilon(\hat{\nu}) - \xi_{q,\nu}|$.

Theorem 2. *For all $n \geq 1$, $q \in (0, 1)$, $L, r > 0$ such that $rL \leq \sup_{x>0} h_q(x)$, it holds that*

$$n = \Omega\left(\frac{C_q^2}{L^2\tau^2} \vee \frac{C_q}{L\tau\epsilon}\right), \quad (2)$$

samples are required for $\mathcal{R}(\epsilon, L, r, q) \leq t$ to hold.

Note that Theorem 2 implies a lower bound on the sample complexity for estimating m quantiles. That is, for all $q = (q_1, \dots, q_m)$, $n \geq 1$, $L, r > 0$ with $rL \leq \inf_{j \in [m]} C_{q_j}$, it holds that (2) samples are also required for $\inf_{T_\epsilon \sim \tilde{\mathcal{M}}_{1,\epsilon,n}(\mathbb{R}^m)} \sup_{\nu \in \mathcal{G}_{L,r,q}} \mathbb{E}\|T_\epsilon(\hat{\nu}) - \xi_{q,\nu}\| \leq t$. Applying this lower bound in conjunction with Theorem 1 yields that the scale and location of the proposed private boxplot are estimated optimally, up to logarithmic factors. Note that Tzamos and Vlatakis-Gkaragkounis (2020) give a minimax lower bound on differentially private median estimation. Their result is similar, though the proof does not directly extend to estimating an arbitrary quantile, since it relies on a set of uniform distributions who have that the property that the median coincides with the mean. The proof of Theorem 2 is an elementary application of the differentially private version of Fano's inequality (Acharya et al., 2021), it is deferred to Appendix A.

Remark 3. Our theoretical exposition is based on `JointExp`, but any algorithm whose quantiles satisfy the same sample complexity bound given by Theorem 1 would result in optimal estimates of location and scale of the boxplot. For instance, `PrivateQuantile` of Smith (2011) is a special case of `JointExp`, when only one quantile is being estimated, and therefore, the same results apply to `PrivateQuantile`. In addition, Lalanne et al. (2023a) give concentration results for the quantiles generated by the algorithm of Kaplan et al. (2022), would also obtain the minimax lower bound given in Theorem 2. Lastly, recall that `JointExp` is inconsistent for estimating extreme quantiles (see Lemma 8). The proof of Lemma 8 also implies that `PrivateQuantile` and `ApproxQuantile` are inconsistent for estimating extreme quantiles.

Next, we show that the whiskers and the outlyingness numbers, when appropriately normalized, are weakly consistent for their population counterparts. We first require a condition on the population measure.

Condition 1. There exists $K, r, L > 0$ such that $\nu \in \mathcal{G}_{L,r,1/4} \cap \mathcal{G}_{L,r,1/2} \cap \mathcal{G}_{L,r,3/4}$ and $\sup_{x \in [a,b]} f_\nu(x) \leq K < \infty$.

Condition 1 requires that the population distribution have a bounded density, which is also bounded below in a neighborhood of the median and the quartiles. For instance, it is easily seen that Condition 1 is satisfied by the Gaussian, student t , Gamma, Beta, and uniform distribution families.

Theorem 4. *For $-\infty < a < b < \infty$, if $\lambda_n \rightarrow 0$ as $n \rightarrow \infty$, Condition 1 holds and $a \leq \xi_{1/4,\nu} < \xi_{3/4,\nu} \leq b$, then, for all non-increasing sequences $\beta_n \rightarrow 1$, it holds that $\tilde{\ell} \xrightarrow{P} \ell_\nu$, $\tilde{u} \xrightarrow{P} u_\nu$, $\tilde{o}_\ell/n \xrightarrow{P} o_{\ell,\nu}$ and $\tilde{o}_u/n \xrightarrow{P} o_{u,\nu}$.*

Theorem 4 implies that for large sample sizes, the skewness and tails will be correctly portrayed by the differentially private boxplot. Together, Theorems 1 and 4 imply that, given a large enough sample size, `DPBoxplot` will correctly represent the location, scale, skewness and tail of the underlying distribution. Thus, making it statistically valid for one to use the private boxplot to describe and compare multiple samples in a differentially private exploratory data analysis.

5 Simulations

We now assess the empirical performance of `DPBoxplot`. We compare `DPBoxplot` to the “naive private boxplot” and the `non-private` sample boxplot. The naive private boxplot is one where a single differentially private quantile algorithm is used to generate all quantiles that are used in the boxplot. Using these quantiles, the whiskers and outlyingness counts are then constructed in the same manner as that of Algorithm 1. We consider the following quantile estimation methods: `PrivateQuantile` (Smith, 2011), `unbounded` (Durfee, 2023), `ApproxQuantile` (Kaplan et al., 2022) and `JointExp` (Gillenwater et al., 2021). For all algorithms, we set $a = -50$ and $b = 50$ and $\lambda_n = n^{-1/4}$. We ran the same simulations with other values of λ_n and found it did not alter the conclusions of the study, see Appendix B.2. The parameter β in the `unbounded` algorithm was set at the default value in both the naive boxplot and `DPBoxplot`.

We assess the boxplots across the four key metrics: scale, location, skewness and tails. We consider the error between each boxplot and the population boxplot. For `DPBoxplot`, the errors in each of the components are quantified as follows: $|\tilde{\xi}_{1/2} - \xi_{1/2,\nu}|$ (location), $|\text{IQR} - \text{IQR}(\nu)|$ (scale), $|\tilde{\ell} - \ell_\nu| + |\tilde{u} - u_\nu|$ (skewness), $|\tilde{o}_\ell - no_{\ell,\nu}| + |\tilde{o}_u - no_{u,\nu}|$ (tails). The errors for the remaining boxplots are defined analogously.

Data were generated from the five distinct distributions parametrized to have mean 0 and variance 1: normal distribution (`normal`), skew normal distribution (`skew`), uniform distribution (`uniform`), beta distribution (`beta`), and an empirical distribution of 2019 NY airbnb listing prices (`airbnb`)³. We considered values of n and ϵ and each scenario was simulated 1000 times. (For more details, see Appendix B.1). Results from `beta` and `airbnb` distributions, and those with $\epsilon = 0.5$ did not add additional insights, so we defer these to Appendix B.1. We also assessed `DPBoxplot`’s ability to compare multiple distributions

³These data were sampled without replacement.

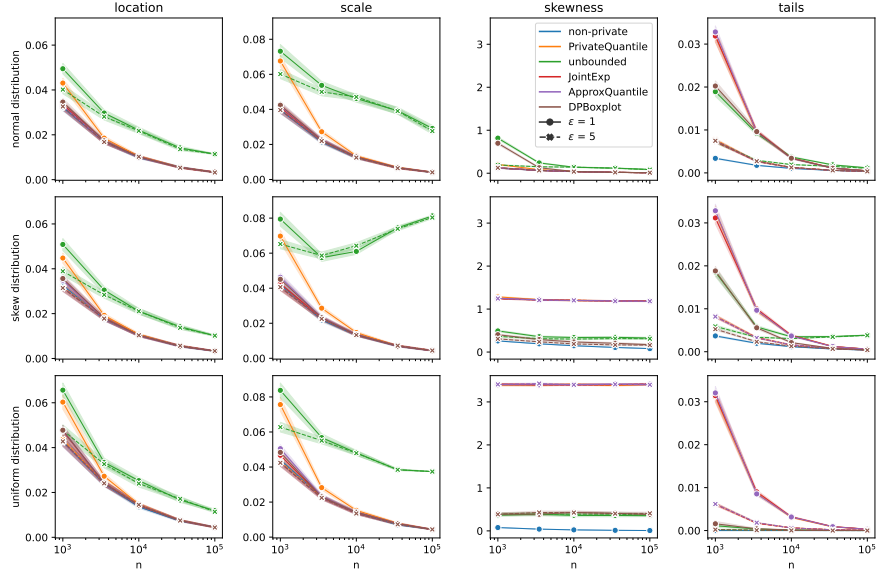


Figure 1: Average error in each metric with 95% confidence intervals between the different differentially private boxplots and their corresponding population boxplot (y-axis) with $\epsilon \in \{1, 5\}$ (line style) and increasing n (x-axis). The DPBoxplot algorithm is presented, along with the naive method paired with each of the algorithms JointExp, ApproxQuantile, unbounded and PrivateQuantile (line color). The non-private line is the distance between the non-private boxplot and its corresponding population boxplot.

simultaneously, concluding that DPBoxplot also performs well under this setting. For brevity, these results are deferred to Appendix B.3.

Figure 1 provides a comprehensive summary of the simulation results. Each column of figures corresponds to a distinct boxplot component, while each row pertains to a different generating distribution. The sample size is depicted along the x -axis, while the average error is represented on the y -axis. The line color within the figures denotes the method used to generate the boxplot and the line style corresponds to the privacy budget ϵ .

Consistent with Theorems 1, 2, and 4, the error for all components of DPBoxplot is converging to zero as n increases in all scenarios. Further, we see that the error for DPBoxplot is similar to that of the error for non-private. This means that the sampling error is larger than that of the error attributed to privatization.

On the other hand, the naive boxplots do not always exhibit the same behavior. In particular, the inconsistency of the whiskers for the naive methods based

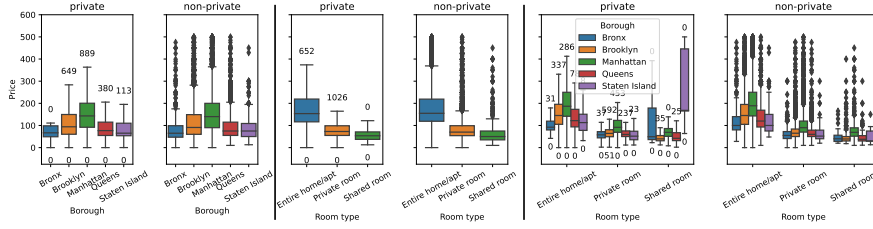


Figure 2: Private and non-private boxplots for inquiry 1. The boxplots display listing prices against borough, room type and room type separated by borough in columns 1, 2 and 3, respectively. Private boxplots are obtained with a total aggregated budget of $\epsilon = 1$.

on `JointExp`, `ApproxQuantile`, and `PrivateQuantile` is reflected empirically through poor performance in the skew metric for the `skew` and `uniform` distributions. On the other hand, though it does well at estimating the extreme quantiles, the `unbounded` algorithm exhibits poor performance in terms of estimating scale and location, relative to the other algorithms. We see that `DPBoxplot` retains the best of both worlds.

In the setting of normally distributed data at small sample sizes, `DPBoxplot` does perform worse than the naive methods in the skewness metric. This happens because at small sample sizes, the `unbounded` algorithm tends to underestimate the magnitude of the minimum and maximum of the dataset, while the other algorithms overestimate the magnitude of the minimum and maximum. Nevertheless, we can still conclude that overall, `DPBoxplot` exhibits consistently better behavior than the naive methods.

6 Case study

We now conduct an exploratory data analysis via boxplots, within the framework of differential privacy. To simulate a real world setting, we enforce a total privacy budget of $\epsilon = 2$. That is, all the private visualizations generated in the case study collectively result in a 2-differentially private release from the dataset. We consider two business inquiries, each with a privacy budget of $\epsilon = 1$. Each inquiry consists of several visualizations. The privacy budget for each visualization is proportional to the number of boxplots in the visualization. To elaborate, out of the total budget ($\epsilon = 1$), each visualization (and therefore, as a result of parallel composition, each boxplot) is assigned a privacy budget equal to the number of boxplots in the visualization, divided by the number of boxplots on all generated visualizations. We chose this allocation so that more budget is allotted to visualizations where the data is partitioned more times. The intuition is that if the data is partitioned more times, then each boxplot in the visualization has a sample size which is smaller. Code for replicating our visualizations has been made publicly accessible .

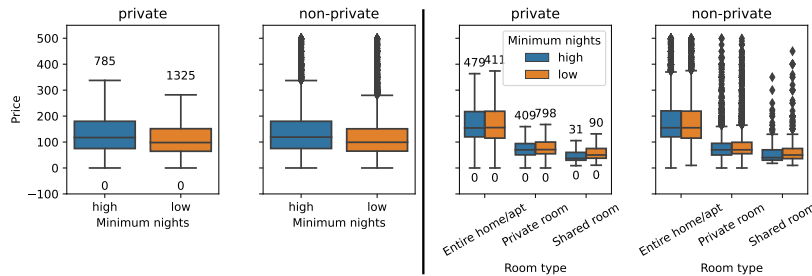


Figure 3: Private and non-private boxplots for inquiry 2. The boxplots display listing prices against minimum nights and room type separated by minimum nights in columns 1 and 2, respectively. Private boxplots are obtained with a total aggregated budget of $\epsilon = 1$.

We analyze a dataset containing Airbnb listing prices and associated metrics within New York City (NYC) in 2019 (Kaggle, 2019). After removing listings priced above 500 US dollars (USD) and requiring minimum nights of stay fewer than 10, this dataset has $n = 40738$ observations and $d = 4$ explanatory variables of business interest. We only consider listings priced below 500 USD, and so we set $a = 0$ and $b = 500$. We address two distinct business inquiries:

Inquiry 1: Do discernible patterns emerge in Airbnb listing prices across various boroughs in New York City and differing room types?

The dataset encompasses five distinct boroughs within New York City, namely Bronx, Brooklyn, Manhattan, Queens, and Staten Island, alongside three offered room types: Entire Home, Private Room, and Shared Room. We present three visualizations: boxplots of prices by borough, by room type, and a combined visualization of prices by borough and room type. These generate 5, 3, and 15 boxplots, respectively, totaling 23.

The differentially private boxplots are displayed in Figure 2, juxtaposed with their non-private counterparts. Only looking at the differentially private boxplots, Figure 2 reveals that prices predominantly lie in the bottom end of the range $[0,500]$, with a right skew and heavy right tail observed across all boroughs and room types, except for in the Bronx, and for shared rooms. The distribution of prices in the Bronx still exhibits a right skew, but has light tails. The distribution of prices for shared rooms appears to be symmetric, with light tails. Notably, prices appear elevated for Manhattan. As expected, entire homes are priced higher than shared spaces. The right-most plot, which displays prices by both borough and room type, affirms previous observations, except shared rooms in Staten Island and the Bronx. Staten Island and the Bronx exhibits higher variability for shared rooms.

It is natural to compare the patterns observed on the differentially private boxplots to those observed in the non-private boxplots. As previously mentioned, Figure 2 juxtaposes the differentially private boxplots with the non-private boxplots. Many conclusions derived from the private visualizations persist in the

non-private domain. However, there are several disparities, which are outlined as follows: In reality, both the listing prices for shared rooms and properties in the Bronx do have a heavy, right tail. The second disparity occurs in the third plot, where the non-private plots does not indicate higher prices and variability for properties in Staten Island and the Bronx in shared rooms. These discrepancies can be explained by small sample sizes and our conservative choice of privacy budget. For instance, the number of shared room listings in Staten Island is only 9.

Inquiry 2: Are there observable trends in Airbnb listing prices concerning minimum nights required for reservation and the types of rooms offered?

We create a new categorical variable called minimum nights, in which a listing is assigned “low” if it has less than or equal to three minimum nights, and “high” otherwise. For this inquiry, we generate two visualizations: Boxplots of prices by minimum nights, and prices by combinations of minimum nights and room offered. These visualizations require 2, and 6 boxplots, respectively, totaling 8.

The differentially private boxplots are displayed in Figure 3, juxtaposed with their non-private counterparts. Again, we first analyze the patterns in the differentially private boxplots, and compare to those observed in the private boxplots afterward. The differentially private boxplots indicate the emergence of a phenomenon akin to Simpson’s paradox. Specifically, a preliminary examination suggests that listings requiring a higher minimum number of nights are priced more steeply than their counterparts with lower minimum requirements. However, this trend disappears when the data is divided by room type. Listings for entire rooms exhibit no significant price differential based on minimum night requirement, while private rooms slightly favor lower minimum nights in terms of price. In shared rooms the median price does not seem to be significantly different.

A comparative analysis with non-private boxplots reaffirms these observations; we observe relatively consistent patterns between the private and non-private boxplots. The primary visual disparity pertains to the positioning of the lower whiskers on the boxplots. This underscores the recognized challenge associated with differentially private estimation of extreme quantiles. However, this discrepancy does not materially impede the analytical value of our findings.

Overall, the patterns observed are generally consistent between the private and non-private boxplots. The principal disparities are attributable to sample size, a factor we encourage practitioners to consider when conducting differentially private exploratory analyses. This case study demonstrates the potential of differentially private, exploratory data analysis and confirms the efficacy of the differentially private boxplot, in accordance with our theoretical and simulated results.

References

- Acharya, J., Sun, Z., and Zhang, H. (2021). Differentially private Assouad, Fano, and Le Cam. In Feldman, V., Ligett, K., and Sabato, S., editors, *Proceedings of the 32nd International Conference on Algorithmic Learning Theory*, volume 132 of *Proceedings of Machine Learning Research*, pages 48–78. PMLR.
- Acs, G., Castelluccia, C., and Chen, R. (2012). Differentially private histogram publishing through lossy compression. In *2012 IEEE 12th International Conference on Data Mining*, pages 1–10. IEEE.
- Alabi, D., Ben-Eliezer, O., and Chaturvedi, A. (2022). Bounded space differentially private quantiles.
- Bhattacharjee, K., Chen, M., and Dasgupta, A. (2020). Privacy-preserving data visualization: Reflections on the state of the art and research opportunities. *Computer Graphics Forum*, 39:675–692.
- Budiu, M., Thaker, P., Gopalan, P., Wieder, U., and Zaharia, M. (2022). Overlook: Differentially private exploratory visualization for big data. *Journal of Privacy and Confidentiality*, 12.
- Dasgupta, A., Chen, M., and Kosara, R. (2013). Measuring privacy and utility in privacy-preserving visualization. *Computer Graphics Forum*, 32:35–47.
- Dasgupta, A. and Kosara, R. (2011). Adaptive privacy-preserving visualization using parallel coordinates. *IEEE Transactions on Visualization and Computer Graphics*, 17(12):2241–2248.
- Dasgupta, A., Kosara, R., and Chen, M. (2019). Guess me if you can: A visual uncertainty model for transparent evaluation of disclosure risks in privacy-preserving data visualization. In *2019 IEEE Symposium on Visualization for Cyber Security (VizSec)*, pages 1–10.
- Durfee, D. (2023). Unbounded differentially private quantile and maximum estimation. In Oh, A., Neumann, T., Globerson, A., Saenko, K., Hardt, M., and Levine, S., editors, *Advances in Neural Information Processing Systems*, volume 36, pages 77691–77712. Curran Associates, Inc.
- Dwork, C. (2008). Differential privacy: A survey of results. In *International conference on theory and applications of models of computation*, pages 1–19. Springer.
- Dwork, C., McSherry, F., Nissim, K., and Smith, A. (2006). Calibrating noise to sensitivity in private data analysis. In *Theory of Cryptography Conference*, pages 265–284.
- Garrido, G. M., Liu, X., Matthes, F., and Song, D. (2023). Lessons learned: Surveying the practicality of differential privacy in the industry. *Proceedings on Privacy Enhancing Technologies*, 2023:151–170.

- Gillenwater, J., Joseph, M., and Kulesza, A. (2021). Differentially private quantiles. In Meila, M. and Zhang, T., editors, *Proceedings of the 38th International Conference on Machine Learning*, volume 139 of *Proceedings of Machine Learning Research*, pages 3713–3722. PMLR.
- Hay, M., Rastogi, V., Miklau, G., and Suci, D. (2010). Boosting the accuracy of differentially private histograms through consistency. *Proc. VLDB Endow.*, 3(1–2):1021–1032.
- He, X., Raval, N., and Machanavajjhala, A. (2016). A demonstration of visdpt. *Proceedings of the VLDB Endowment*, 9:1489–1492.
- Hongde, R., Shuo, W., and Hui, L. (2014). Differential privacy data aggregation optimizing method and application to data visualization. In *2014 IEEE Workshop on Electronics, Computer and Applications*, pages 54–58.
- Ji, Z., Lipton, Z. C., and Elkan, C. (2014). Differential privacy and machine learning: a survey and review.
- Kaggle (2019). New york city airbnb open data.
- Kaplan, H., Schnapp, S., and Stemmer, U. (2022). Differentially private approximate quantiles. In Chaudhuri, K., Jegelka, S., Song, L., Szepesvari, C., Niu, G., and Sabato, S., editors, *Proceedings of the 39th International Conference on Machine Learning*, volume 162 of *Proceedings of Machine Learning Research*, pages 10751–10761. PMLR.
- Kellaris, G. and Papadopoulos, S. (2013). Practical differential privacy via grouping and smoothing. *Proceedings of the VLDB Endowment*, 6(5):301–312.
- Lalanne, C., Garivier, A., and Gribonval, R. (2023a). Private statistical estimation of many quantiles. In Krause, A., Brunskill, E., Cho, K., Engelhardt, B., Sabato, S., and Scarlett, J., editors, *Proceedings of the 40th International Conference on Machine Learning*, volume 202 of *Proceedings of Machine Learning Research*, pages 18399–18418. PMLR.
- Lalanne, C. S., Gastaud, C., Grislain, N., Garivier, A., and Gribonval, R. (2023b). Private quantiles estimation in the presence of atoms.
- Li, C., Hay, M., Rastogi, V., Miklau, G., and McGregor, A. (2010). Optimizing linear counting queries under differential privacy. In *Proceedings of the twenty-ninth ACM SIGMOD-SIGACT-SIGART symposium on Principles of database systems*, pages 123–134.
- Liu, W., Zhang, Y., Yang, H., and Meng, Q. (2023). A survey on differential privacy for medical data analysis. *Annals of Data Science*, 11(2):733–747.
- Nanayakkara, P., Bater, J., He, X., Hullman, J., and Rogers, J. (2022). Visualizing privacy-utility trade-offs in differentially private data releases. *Proceedings on Privacy Enhancing Technologies*, 2022:601–618.

- Panavas, L., Crnovrsanin, T., Adams, J. L., Ullman, J., Sargavad, A., Tory, M., and Dunne, C. (2024). Investigating the visual utility of differentially private scatterplots. *IEEE Transactions on Visualization and Computer Graphics*, pages 1–16.
- Ramsay, K., Jagannath, A., and Chenouri, S. (2024). Differentially private multivariate medians.
- Smith, A. (2011). Privacy-preserving statistical estimation with optimal convergence rates. In *Proceedings of the forty-third annual ACM symposium on Theory of computing, STOC’11*. ACM.
- Tukey, J. W. et al. (1977). *Exploratory data analysis*, volume 2. Springer.
- Tzamos, C. and Vlatakis-Gkaragkounis (2020). Optimal private median estimation under minimal distributional assumptions. In Larochelle, H., Ranzato, M., Hadsell, R., Balcan, M., and Lin, H., editors, *Advances in Neural Information Processing Systems*, volume 33, pages 3301–3311.
- Xu, J., Zhang, Z., Xiao, X., Yang, Y., Yu, G., and Winslett, M. (2013). Differentially private histogram publication. *The VLDB journal*, 22:797–822.
- Zhang, D., Hay, M., Miklau, G., and O’connor, B. (2016). Challenges of visualizing differentially private data.
- Zhang, X., Chen, R., Xu, J., Meng, X., and Xie, Y. (2014). Towards accurate histogram publication under differential privacy. pages 587–595. Society for Industrial and Applied Mathematics.
- Zhou, J., Wang, X., Wong, J. K., Wang, H., Wang, Z., Yang, X., Yan, X., Feng, H., Qu, H., Ying, H., and Chen, W. (2022). Dpviscreator: Incorporating pattern constraints to privacy-preserving visualizations via differential privacy. *IEEE Transactions on Visualization and Computer Graphics*, pages 1–11.

A Technical proofs

Before presenting the proof of Theorem 1, we first prove a general sample complexity bound for quantiles. For $t \geq 0$, $q = (q_1, \dots, q_m)$ such that $0 < q_1 < \dots < q_m < 1$, $-\infty < a < b < \infty$, and $\nu \in \mathcal{M}_1(\mathbb{R})$, define:

$$\alpha(t) = \inf_{a < x_1 < \dots < x_m < b, \|x - \xi_{q,\nu}\| \geq t} \sum_{i=1}^{m+1} |q_j - q_{j-1} - F_\nu(x_j) + F_\nu(x_{j-1})|.$$

One may wish to recall that $\inf \emptyset = \infty$, and so $\alpha(t)$ is still defined if $\{a < x_1 < \dots < x_m < b, \|x - \xi_{q,\nu}\| \geq t\} = \emptyset$.

Lemma 5. *For $-\infty < a < b < \infty$, if $\nu \in \mathcal{M}_1(\mathbb{R})$ is absolutely continuous such that $\sup_{x \in [a,b]} f_\nu(x) \leq K < \infty$, then there exists universal constants $C, c > 0$ such that for all $q = (q_1, \dots, q_m)$ such that $0 < q_1 < \dots < q_m < 1$ and $a \leq \xi_{q_1,\nu} \leq \dots \leq \xi_{q_m,\nu} \leq b$, all $t \geq 0$ and $0 < \gamma < 1$, it holds that $\|\xi_{q,\tilde{\nu}} - \xi_{q,\nu}\| \leq t$, with probability $1 - \gamma$, provided that*

$$n \geq Cm^2 \frac{\log(1/\gamma) \vee m \log m / c\alpha(t)}{\alpha^2(t)} \bigvee m \frac{\log(1/\gamma) \vee \log\left(\frac{K(b-a)}{q_1 \wedge (1-q_m) \wedge \alpha(t)}\right)}{\alpha(t)\epsilon}. \quad (3)$$

Proof of Lemma 5. Given that $\tilde{\xi}_{q,\tilde{\nu}}$ is a draw from the exponential mechanism, the result follows from an application of Corollary 7 of Ramsay et al. (2024). Corollary 7 of Ramsay et al. (2024) gives an upper bound on the sample complexity of a draw from the exponential mechanism, provided the utility function meets certain criteria. In order to apply Corollary 7 of Ramsay et al. (2024), we must show that the following function

$$\begin{aligned} \phi'(x, \nu) &= - \sum_{j=1}^{m+1} |F_\nu(x_j) - F_\nu(x_{j-1}) - (q_j - q_{j-1})| \mathbb{1}\{[x_1, x_m] \in [a, b]\} \\ &\quad - \infty \cdot (1 - \mathbb{1}\{[x_1, x_m] \in [a, b]\}), \end{aligned}$$

and ν satisfy three conditions. First, we must show that $\phi'(x, \nu)$ has a maximum, which is easily seen by definition, $\phi'(x, \nu)$ is maximized at $\xi_{q,\nu}$. The second requirement is that $\phi'(x, \nu)$ is K -Lipschitz, which follows by assumption. Lastly, Corollary 7 of Ramsay et al. (2024) requires that $\phi'(x, \nu)$ is a (L, \mathcal{F}) regular function for some $L > 0$ with $\text{VC}(\mathcal{F}) < \infty$, see Definition 2. It is easy to see that $\phi'(x, \nu)$ is (m, \mathcal{F}) regular function with $\text{VC}(\mathcal{F}) = 1$. In order to apply the bound given in Corollary 7 of Ramsay et al. (2024), we must compute the discrepancy function of ϕ', ν , which is given by: $\alpha'(t) = \phi'(\xi_{q,\nu}, \nu) - \sup_{\|x - \xi_{q,\nu}\| \geq t} \phi'(x, \nu)$. A straightforward calculation yields that $\alpha'(t) = \alpha(t)$. Applying Corollary 7 of Ramsay et al. (2024), yields that there exists a universal constant $C > 0$ such that for any $t > 0$ and $0 \leq \gamma \leq 1$, $\|\xi_{q,\tilde{\nu}} - \xi_{q,\nu}\| \leq t$ with probability at least $1 - \gamma$, if

$$n \geq C \left(m^2 \frac{\log(1/\gamma) \vee m \log m / c\alpha(t)}{\alpha^2(t)} \bigvee m \frac{\log(1/\gamma) \vee \log\left(\frac{(b-a)}{|\xi_{q_1,\nu} - a| \wedge |b - \xi_{q_m,\nu}| \wedge \alpha(t)/K}\right)}{\alpha(t)\epsilon} \right).$$

Define $a \gtrsim b$ ($a \lesssim b$) if there is a universal constant $c > 0$ such that $a \geq cb$ ($a \leq cb$). Next, using the Lipschitz assumption and the mean value theorem, we have that $|\xi_{q_1, \nu} - a| \wedge |b - \xi_{q_m, \nu}| \gtrsim [q_1 \wedge (1 - q_m)]/K$, which yields the desired result. \square

We can now prove Theorem 1.

Proof of Theorem 1. The proof is based on an application of Lemma 5. All of the conditions of Lemma 5 are satisfied by assumption, and so it remains to lower bound α . To this end, let $k_x = \operatorname{argmax}_{i \in [m]} |x_i - \xi_{q_i, \nu}|$. Using this notation, for $0 \leq t \leq r$, the definition of α in conjunction with the mean value theorem yields that

$$\begin{aligned} \alpha(t) &= \inf_{a < x_1 < \dots < x_m < b, \|x - \xi_{q, \nu}\| \geq t} \sum_{j=1}^{m+1} |q_j - q_{j-1} - F_\nu(x_j) + F_\nu(x_{j-1})| \\ &\geq \inf_{a < x_1 < \dots < x_m < b, \|x - \xi_{q, \nu}\| \geq t} \sum_{j=1}^{k_x} |q_j - q_{j-1} - F_\nu(x_j) + F_\nu(x_{j-1})| \\ &\geq \inf_{a < x_1 < \dots < x_m < b, \|x - \xi_{q, \nu}\| \geq t} \left| \sum_{j=1}^{k_x} q_j - q_{j-1} - F_\nu(x_j) + F_\nu(x_{j-1}) \right| \\ &\geq \inf_{a < x_1 < \dots < x_m < b, \|x - \xi_{q, \nu}\| \geq t} |q_{k_x} - F_\nu(x_{k_x})| \\ &\geq tL/\sqrt{m}. \end{aligned}$$

Applying this bound, in conjunction with Lemma 5, yields the desired result. \square

Next, we prove Theorem 2.

Proof of Theorem 2. We apply Corollary 4 of (Acharya et al., 2021), of which a simpler version is restated below for clarity. For $\mathcal{P} \subset \mathcal{M}_1(\mathbb{R})$, let $n^* = \inf\{n: \inf_{T_\epsilon \sim \tilde{\mathcal{M}}_{1, \epsilon, n}(\mathbb{R})} \sup_{\nu \in \mathcal{P}} \int |T_\epsilon(\hat{\nu}) - T_\epsilon(\nu)| d\nu^n \leq \tau\}$.

Corollary 6 (Acharya et al. (2021)). *For all $\epsilon, \tau > 0$ and any $\mathcal{P} \subset \mathcal{M}_1(\mathbb{R})$, let $\mathcal{Q} = \{Q_1, \dots, Q_m\} \subset \mathcal{P}$. If for all $i \neq j$, it holds that $|T_\epsilon(Q_i) - T_\epsilon(Q_j)| \geq 3\tau$, $\text{KL}(Q_i, Q_j) \leq \beta_n$, and $\text{TV}(Q_i, Q_j) \leq \gamma$, then $n^* = \Omega(\log m(\beta_n^{-1} \vee (\gamma\epsilon)^{-1}))$.*

In order to apply Corollary 6, we first define a class of Gaussian measures which lie in $\mathcal{G}_{L, r, q}$. Recall that we consider ν with densities which satisfy: $\inf_{x \in \xi_{q, \nu} \pm r} f_\nu(x) \geq L$. Let $P_{\mu, \sigma} = \mathcal{N}(\mu, \sigma^2)$ and let $h_{\mu, \sigma}$ denote the associated quantile function. We have that for $q \leq 1/2$, it holds that

$$\begin{aligned} \inf_{x \in h_{\mu, \sigma}(q) \pm r} f_{P_{\mu, \sigma}}(x) &\geq (2\pi\sigma^2)^{-1/2} \exp\left(-[\operatorname{erf}^{-1}(2q-1) - r/\sqrt{2}\sigma]^2\right) \\ &\geq (2\pi\sigma^2)^{-1/2} \exp\left(-r^2/2\sigma^2 - [\operatorname{erf}^{-1}(2q-1)]^2\right). \end{aligned}$$

Taking $\sigma = C_q/\sqrt{2\pi}L$ gives that

$$\inf_{x \in h_{\mu, \sigma}(q) \pm r} f_{P_{\mu, \sigma}}(x) \geq L/C_q \exp\left(-[\operatorname{erf}^{-1}(2q-1)]^2 - \pi r^2 L^2/C_q^2\right).$$

Now, note that

$$\operatorname{erf}^{-1}(2q-1) = \Phi^{-1}(q)/\sqrt{2},$$

which in turn implies that

$$\inf_{x \in h_{\mu, \sigma}(q) \pm r} f(x) \geq L \exp\left(-[\Phi^{-1}(q)]^2/2 - r^2 L^2\right)/\sqrt{\pi}.$$

Next, we have that

$$\begin{aligned} L/C_q \exp\left(-[\Phi^{-1}(q)]^2/2 - \pi r^2 L^2/C_q^2\right) &\geq L \\ &\iff \exp\left(-[\Phi^{-1}(q)]^2/2 - \pi r^2 L^2/C_q^2\right) \geq C_q \\ &\iff [\Phi^{-1}(q)]^2/2 + \pi r^2 L^2/C_q^2 \leq -\log C_q \\ &\iff rL \leq C_q \sqrt{(-\log C_q - [\Phi^{-1}(q)]^2/2)/\pi}. \end{aligned}$$

We must then have that $rL \leq C_q \sqrt{(-\log C_q - [\Phi^{-1}(q)]^2/2)/\pi}$, which holds by assumption. Define $\mathcal{F}_{L,r} = \{\mathcal{N}(\mu, C_q^2/2\pi L^2) : \mu \in \mathbb{R}\}$. We find the values of β_n, γ and τ for $\mathcal{F}_{L,r}$. Consider the values μ_0, μ_1 , and for $i=1$ or $i=0$, denote $Q_i = P_{\mu_i, C_q^2/2\pi L^2}$. Note that for any quantile q , we have that $|\xi_{q, Q_0} - \xi_{q, Q_1}| = |\mu_0 - \mu_1|$. That is, the distance between the quantiles is just the difference between the means. For some $\tau > 0$, take any μ_0, μ_1 such that $|\mu_0 - \mu_1| \geq 3\tau$. It follows that $\operatorname{KL}(Q_0, Q_1) \lesssim \tau^2 L^2/C_q^2$ and $\operatorname{TV}(Q_0, Q_1) = 2\Phi(c\tau L/C_q) - 1 \lesssim L\tau/C_q$. Therefore, applying Corollary 6 gives that

$$n^* = \Omega\left(\frac{C_q^2}{L^2\tau^2} \vee \frac{C_q}{L\tau\epsilon}\right). \quad \square$$

Before proceeding with the proof of Theorem 4, we first prove that the unbounded algorithm estimates extreme quantiles consistently.

Lemma 7. *For all non-increasing sequences $\beta_n \rightarrow 1$ and $q_n \rightarrow 0$, and all $\nu \in \mathcal{M}(\mathbb{R})$, it holds that*

$$i \text{ if } \min(\nu) < b, \text{ then } \tilde{\psi}_{q_n} \xrightarrow{P} \min(\nu).$$

$$ii \text{ if } \max(\nu) > a, \text{ then } \tilde{\psi}_{1-q_n} \xrightarrow{P} \max(\nu).$$

Proof. First, without loss of generality, take $a = 0$. Next, using the fact that V_0 is a standard exponential random variable.

$$\Pr(2V_0/n\epsilon > 1 - q_n) = e^{-n(1-q_n)\epsilon/2}. \quad (4)$$

In addition, letting $c_n = 1/\log n$, the Dvoretzky–Kiefer–Wolfowitz inequality yields that

$$\Pr\left(\sup_{x \in \mathbb{R}} |F_{\tilde{\nu}}(x) - F_{\nu}(x)| > c_n\right) \leq 2e^{-2n/(\log n)^2}. \quad (5)$$

It suffices to show that for all $t > 0$, it holds that $\Pr\left(|\tilde{\psi}_{1-q_n} - \max(\nu)| > t\right) \rightarrow 0$ as $n \rightarrow \infty$. (A symmetric argument then implies that also, $\Pr\left(|\tilde{\psi}_{q_n} - \min(\nu)| > t\right) \rightarrow 0$ as $n \rightarrow \infty$.) Letting k be the integer such that $\tilde{\psi}_{1-q_n} = \beta_n^k - 1$, we have that

$$\Pr\left(|\tilde{\psi}_{1-q_n} - \max(\nu)| > t\right) = \Pr\left(\max(\nu) - \beta_n^k - 1 > t\right) + \Pr\left(\beta_n^k - 1 - \max(\nu) > t\right),$$

for which we can write

$$\begin{aligned} \Pr\left(\max(\nu) - \beta_n^k - 1 > t\right) &= \Pr\left(k < \frac{\log(\max(\nu) - t - 1)}{\log \beta_n}\right) := \Pr(k < R_{t,1}), \\ \Pr\left(\beta_n^k - 1 - \max(\nu) > t\right) &= \Pr\left(k > \frac{\log(\max(\nu) + t + 1)}{\log \beta_n}\right) := \Pr(k > R_{t,2}). \end{aligned}$$

It suffices to show that $\Pr(k < R_{t,1}), \Pr(k > R_{t,2}) \rightarrow 0$ as $n \rightarrow \infty$. To this end, first, note that if

$$\frac{\log(\max(\nu) + t + 1)}{\log \beta_n} - \frac{\log(\max(\nu) - t - 1)}{\log \beta_n} < 1,$$

then $\Pr(\{k < R_{t,1}\} \cup \{k > R_{t,2}\}) = 1$. However, we have that β_n is decreasing to 1. This immediately implies that for all $t > 0$, there exists $n_0 > 1$ such that for all $n > n_0$, we have that

$$\frac{\log(\max(\nu) + t + 1)}{\log \beta_n} - \frac{\log(\max(\nu) - t - 1)}{\log \beta_n} > 1.$$

Next, utilizing (5), the fact that $V_0 > 0$ and the definition of V_i , we have that

$$\begin{aligned} \Pr(k < R_{t,1}) &= 1 - \prod_{i=1}^{R_{t,1}} \Pr\left(F_{\tilde{\nu}}(\beta_n^i - 1) + 2V_i/n\epsilon < 1 - q_n + 2V_0/n\epsilon\right) \\ &\leq 1 - \prod_{i=1}^{R_{t,1}} \Pr\left(F_{\nu}(\beta_n^i - 1) + 2V_i/n\epsilon < 1 - q_n - c_n\right) + 2e^{-2n/(\log n)^2} \\ &\leq 1 - \prod_{i=1}^{R_{t,1}} \left(1 - \exp\left(-n\epsilon(1 - q_n - c_n - F_{\nu}(\beta_n^i - 1))/2\right)\right) + 2e^{-2n/(\log n)^2} \\ &:= 1 - I + 2e^{-2n/(\log n)^2}. \end{aligned} \quad (6)$$

Now, using the fact that $(1 + x/n)^n \geq 1 + x$ for all $n \geq 1$ and $|x| \leq n$, we have

that

$$\begin{aligned}
I &= \prod_{i=1}^{R_{t,1}} \left(1 - \exp\left(-n\epsilon(1 - q_n - c_n - F_\nu(\beta_n^i - 1))/2\right)\right) \\
&\geq \left(1 - \exp\left(-n\epsilon(1 - q_n - c_n - F_\nu(\beta_n^{R_{t,1}} - 1))/2\right)\right)^{R_{t,1}} \\
&\geq 1 - R_{t,1} \exp\left(-n\epsilon(1 - q_n - c_n - F_\nu(\beta_n^{R_{t,1}} - 1))/2\right).
\end{aligned}$$

Now, applying the preceding inequality in conjunction with (6) yields that

$$\Pr(k < R_{t,1}) \leq R_{t,1} \exp\left(-n\epsilon(1 - q_n - c_n - F_\nu(\beta_n^{R_{t,1}} - 1))/2\right) + 2e^{-2n/(\log n)^2} \rightarrow 0,$$

as $n \rightarrow \infty$. On the other hand, for the term $\Pr(k > R_{t,2})$, utilizing (4) and (5), we have that

$$\begin{aligned}
\Pr(k > R_{t,2}) &\leq \prod_{i=1}^{R_{t,2}} \Pr\left(F_\nu(\beta_n^i - 1) + 2V_i/n\epsilon < 1 - q_n/2 + c_n\right) + 2e^{-2n/(\log n)^2} + e^{-n\epsilon(1-q_n)/2} \\
&\leq \Pr\left(F_\nu(\beta_n^{R_{t,2}} - 1) + 2V_{R_{t,2}}/n\epsilon < 1 - q_n/2 + c_n\right) + 2e^{-2n/(\log n)^2} + e^{-n\epsilon(1-q_n)/2} \\
&\leq \mathbb{1}\left\{1 - q_n/2 + c_n - F_\nu(\beta_n^{R_{t,2}} - 1) \geq 0\right\} + 2e^{-2n/(\log n)^2} + e^{-n\epsilon(1-q_n)/2} \rightarrow 0,
\end{aligned}$$

as $n \rightarrow \infty$. □

We can now prove Theorem 4.

Proof of Theorem 4. We first prove that the whiskers are consistent. Theorem 1 implies that $\tilde{\ell}_1 \xrightarrow{P} \ell_{1,\nu}$ and Lemma 7 implies that $\tilde{\ell}_2 \xrightarrow{P} \min(\nu)$. Continuous mapping theorem and the fact that $\lambda_n \rightarrow 0$ as $n \rightarrow \infty$ yields that $\tilde{\ell} \xrightarrow{P} \ell_\nu$. The same argument applies to the upper whisker.

For the outlyingness number, first, we have that $|o_{\ell,\nu}/n - \tilde{o}_\ell| \leq |o_{\ell,\hat{\nu}} - \tilde{o}_\ell/n| + |o_{\ell,\nu} - o_{\ell,\hat{\nu}}| := I + II$. Next, the properties of the Laplace distribution give that $\Pr(|o_{\ell,\hat{\nu}} - \tilde{o}_\ell/n| \geq t) \lesssim e^{-n\epsilon t}$. Therefore $I \xrightarrow{P} 0$. Next, using the fact that $\sup_{x \in \mathbb{R}} f_\nu(x) \leq K$, we have that F_ν is K -Lipschitz. It follows that $|o_{\ell,\nu}/n - o_{\ell,\hat{\nu}}/n| \leq K|\ell_{\hat{\nu}} - \ell_\nu| + \sup_{x \in \mathbb{R}} |F_\nu(x) - F_{\hat{\nu}}(x)|$. Next, the Dvoretzky–Kiefer–Wolfowitz inequality yields that $\sup_{x \in \mathbb{R}} |F_\nu(x) - F_{\hat{\nu}}(x)| \xrightarrow{P} 0$ and the fact that the whiskers are consistent implies that $K|\ell_{\hat{\nu}} - \ell_\nu| \xrightarrow{P} 0$. The same argument can be made for the upper outlyingness number. □

B Simulation details and additional results

B.1 Single boxplot estimation

This section presents more details on the simulation study described in Section 5. We simulated data from five distributions, each with mean 0 and variance 1: standard normal distribution (`normal`), skew normal distribution with scale parameter 20 (`skew`), uniform distribution with interval $[-\sqrt{3}, \sqrt{3}]$

(**uniform**), a normalized and mean-centered version of the beta distribution with $\alpha = \beta_n = 2$ (**beta**), and normalized and mean-centered empirical distribution generated from 2019 NY airbnb listing prices. We considered sample sizes of $n \in \{1000, 3500, 10000, 35000, 100000\}$ and privacy budgets of $\epsilon \in \{0.5, 1, 5, 10\}$. Each scenario was simulated 1000 times, leading to simulated data vectors \mathbf{X}_n . For each generated dataset, we computed both the non-private boxplot $B(\mathbf{X}_n) = B(\hat{\nu})$ and the population boxplot. We also calculated differentially private boxplots $\tilde{B}(\mathbf{X}_n, \epsilon)$ using each of the methods. Figure 4 is analogous to the Figure 1 in the manuscript, except under more stringent privacy budgets, specifically with $\epsilon = 0.5$ and $\epsilon = 1$. As anticipated, the performance of all methods decreases with lower ϵ values, reflecting the trade-off between privacy and accuracy. However, the decline in performance is marginal, and the same conclusions as those given in Section 5 hold across both privacy levels. In addition, we present Figures 5 and 6, which give a comprehensive summary of the results for `DPBoxplot` from this simulation study.

B.2 Parameter tuning

We performed simulations under similar settings as those discussed in Section B.1. We varied $\lambda_n \in \{n^{-1/2}, n^{-1/4}, 1\}$, fixing $\epsilon = 1$ and estimated differentially private boxplots with all methods. Figure 7 summarizes the results for simulated distributions (column-wise), boxplot metrics (row-wise). Variations in the method and λ_n and are represented with different line colors and line styles, respectively. We observe that none of the methods are highly sensitive to the chosen parameters, except for skewness and tails. Moreover, `DPBoxplot` was generally the best regardless of λ_n . Based on this observation and to account for better results in small samples, we concluded that $\lambda_n = n^{-1/4}$ was a reasonable choice for all methods.

B.3 Multiple boxplot estimation

This section presents an extensive simulation study to assess the differentially private boxplot’s ability to describe, and facilitate comparison of multiple samples. Specifically, we analyze whether the metrics (quantified by distances on location, scale, skewness and tails as in Section 5) between differentially private boxplots across distinct datasets mirror the corresponding pairwise distances observed between their population counterparts. The similitude between two distinct differentially private boxplots is anticipated to align closely with the similitude observed between their respective population counterparts, thereby facilitating analogous visual comparisons and interpretation. For the purpose of quantifying this phenomenon, we introduce the concept of relative similitude between two differentially private boxplots as follows:

$$\tilde{d}\left(\tilde{B}(\mathbf{X}_n, \epsilon), \tilde{B}(\mathbf{Y}_m, \epsilon)\right) = \left| 1 - \frac{d\left(\tilde{B}(\mathbf{X}_n, \epsilon), \tilde{B}(\mathbf{Y}_m, \epsilon)\right) + 1}{d(B(\nu_X), B(\nu_Y)) + 1} \right|.$$

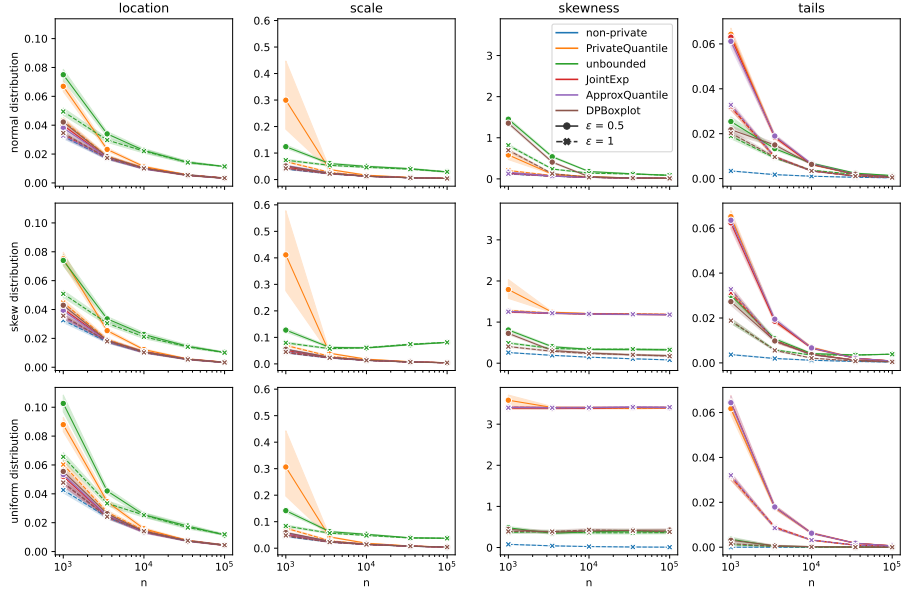


Figure 4: Average error in each metric with 95% confidence intervals between the different differentially private boxplots and their population (**oracle**) counterparts (y-axis) with $\epsilon \in \{0.5, 1\}$ (line style) and increasing n (x-axis). The **DPBoxplot** algorithm is presented, along with the naive method paired with each of the algorithms **JointExp**, **ApproxQuantile**, **unbounded** and **PrivateQuantile** (line color). The different generated distributions are represented row-wise, and the different metrics: location, scale, skewness and tails are presented column-wise. The **non-private** line is the distance between the non-private boxplot and its population counterpart.

Here, distance is related to the four metrics previously described. In order to empirically validate the consistency of our proposed approach with this behavior, we conducted Monte Carlo simulations by generating t datasets $(\mathbf{z}_1, \mathbf{z}_2, \dots, \mathbf{z}_t)$, and two vectors \mathbf{m} and \mathbf{s} of size t sampling from uniform distributions with interval $[-1, 1]$ and $[0.5, 2]$, respectively. Each vector \mathbf{z}_i is size n_i for $i \in \{1, 2, \dots, t\}$ where n_i is chosen randomly such that $n = n_1 + n_2 + \dots + n_t$. Here, t plays the role of the number of treatments in an experiment. We replicated this simulation 1000 times for each combination of $t \in \{4, 8\}$ and $n \in \{500, 5000, 50000\}$ leading to datasets $(\mathbf{X}_1, \mathbf{X}_2, \dots, \mathbf{X}_t)$ such that $\mathbf{X}_i = s_i \mathbf{z}_i + m_i$. We performed this simulation generating the initial t datasets using mixture of the five distributions described in the previous section such that each distribution generates the same amount of vectors on each replica. For each dataset we calculated non-private boxplots $B(\mathbf{X}_1), B(\mathbf{X}_2), \dots, B(\mathbf{X}_t)$, and differentially private boxplots using each of the quantile estimation methods and for each $\epsilon \in \{0.5, 1, 5, 10\}$. We then calculated pair-wise relative boxplot distances for every pair of differentially

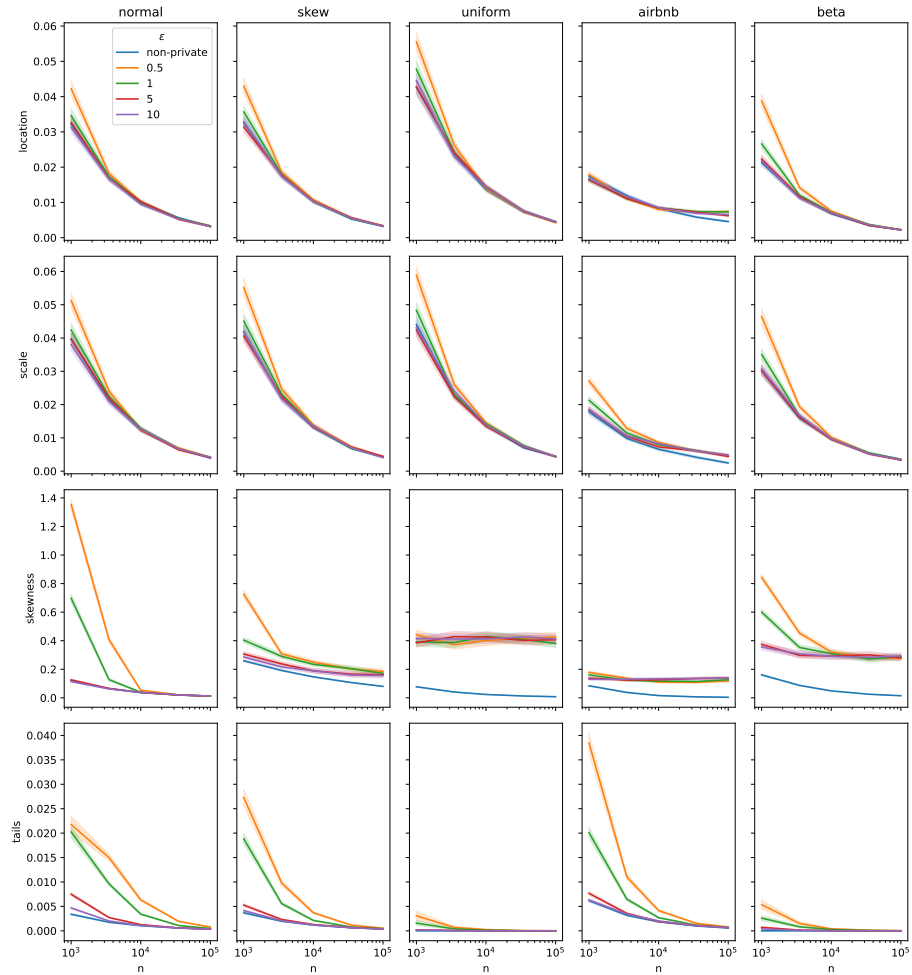


Figure 5: Average error in each metric with 95% confidence intervals between estimated differentially private boxplots and **oracle** boxplot (y-axis) with $\epsilon \in \{0.5, 1, 5, 10\}$ (line colors) and increasing n (x-axis); using **DPBoxplot** for private boxplot estimation; from all sampled distributions (column-wise) comparing location, scale, skewness and tails (row-wise). In the legend, **non-private** refers to the distance between the non-private boxplot and the population boxplot.

private boxplots.

Figure 8 and 9 offers a detailed overview of the results obtained from various scenarios considered. Each boxplot within these plots represents the average pairwise distances observed among all differentially private boxplots generated in a specific scenario. The x -axis on each plot denotes the sample size (n). Variations in hue color correspond to different methods and different privacy budgets (ϵ),

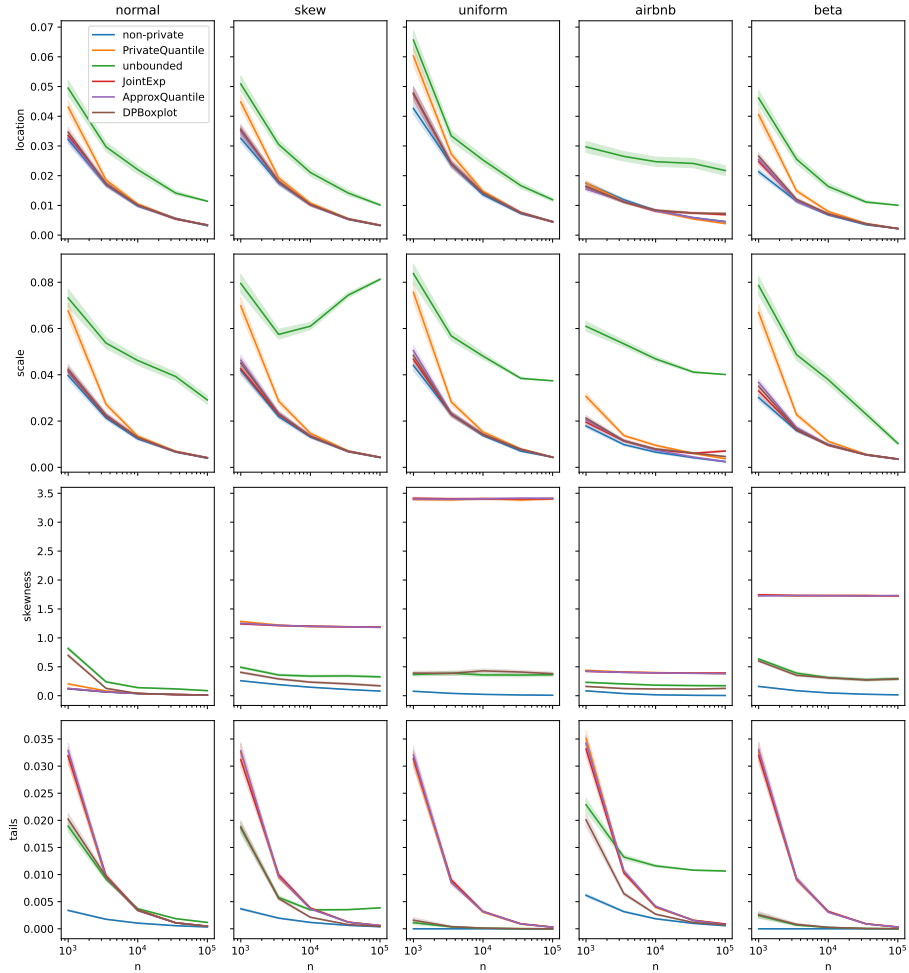


Figure 6: Average error in each metric with 95% confidence intervals between estimated differentially private boxplots and `oracle` boxplots (y-axis) with $\epsilon = 1$ and increasing n (x-axis); using boxplot estimation methods `JointExp`, `ApproxQuantile`, `unbounded`, `PrivateQuantile`, and `DPBoxplot` (line colors); from all sampled distributions (column-wise) comparing location, scale, skewness and tails (row-wise). In the legend, `non-private` refers to the distance between the non-private boxplot and the population boxplot.

respectively. The first and last two plots in the first row correspond to relative location and relative scale, respectively. The first and last two plots in the second row correspond to relative skewness and relative outliers, respectively. For each pair of relative distance plots, the first and second visualization correspond to $t = 5$ and $t = 10$, respectively. Figure 9 uses $\epsilon = 1$ and Figure 8 shows results

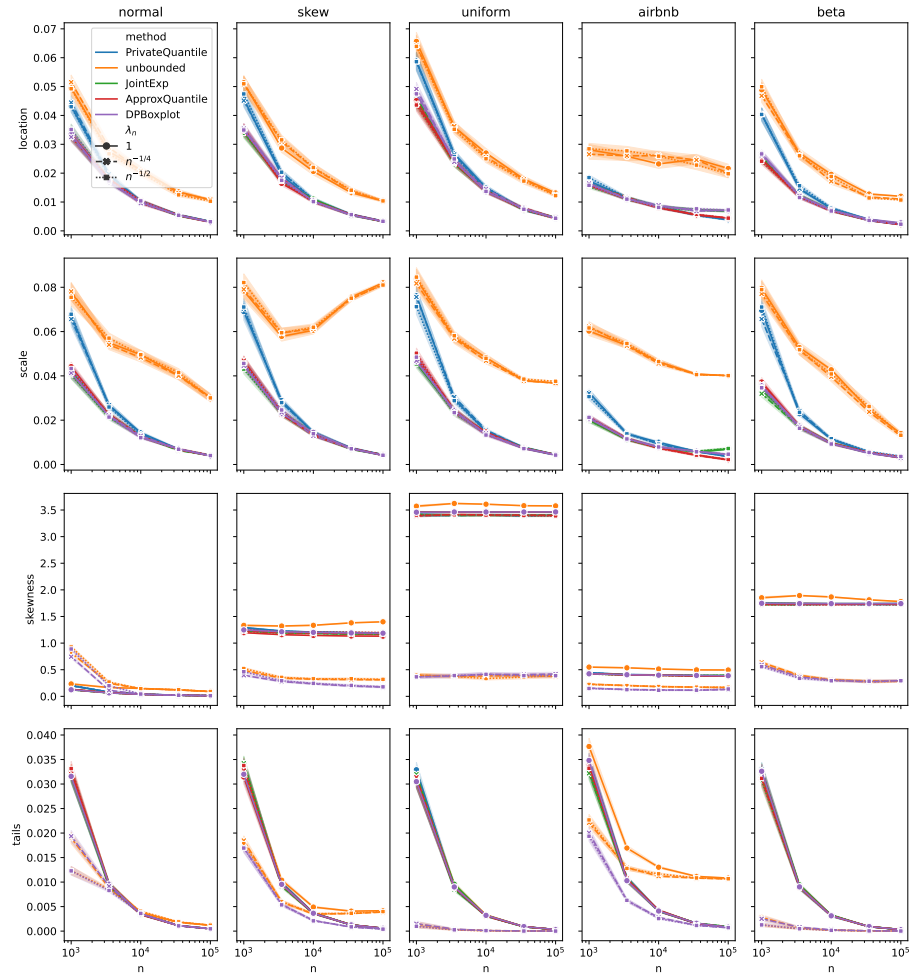


Figure 7: Average error in each metric with 95% confidence intervals between estimated differentially private boxplots (y-axis) and `oracle` boxplots with $\epsilon = 1$ and increasing n (x-axis); using various methods (color), with varying λ_n (line style); from all sampled distributions (column-wise) comparing location, scale, skewness and tails (row-wise).

with `DPBoxplot` method.

Figure 8 shows that `DPBoxplot` performs consistently well across different scenarios. All other methods have poor performance in at least one scenario. In Figure 9 relative distances exhibit a diminishing trend with augmented sample sizes and ϵ , consistent with expectations illustrated by the `non-private` boxplot. A marginal increase in the parameter t leads to a slight augmentation in the relative distances, attributable to the partitioning of data into smaller subsets

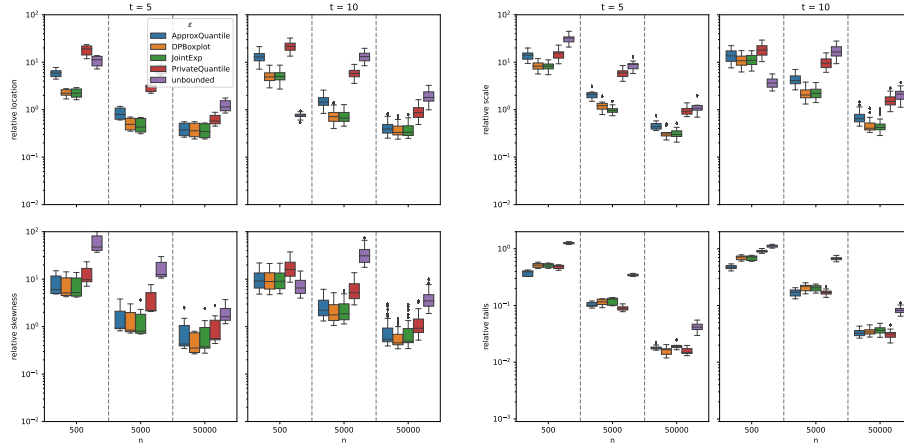


Figure 8: Average pair-wise relative boxplot distances (y-axis) between multiple sample boxplots in terms of relative location, scale, skewness and outliers, with $\epsilon = 1$ using different boxplot estimations (color), $n \in \{500, 5000, 50000\}$ (x-axis) and $t \in \{5, 10\}$ (columns). Legend **non-private** is the relative similitude of the non-private boxplots.

and consequent reduction in sample sizes; however, this impact appears to be negligible. Hence, our analysis suggests that our proposed methodology effectively maintains the visual coherence of relative similarities among diverse boxplots during the execution of multiple comparisons.

B.4 Computational requirements

All simulations were conducted on a single CPU and did not require significant computational resources. The execution time for the simulations presented in the paper did not exceed 24 hours.

C Auxiliary results

The next lemma says that **JointExp** is inconsistent for $q_n = O(1/n)$ if the input bounds do not exactly match those of the support of the population distribution.

Lemma 8. *For $-\infty < a < b < \infty$, if there exists $M > a$ such that $\nu(\{X \leq M\}) = 0$, then for any $0 < t < M - a$, we have that*

$$\Pr\left(|\tilde{\xi}_{q_n} - \xi_{q_n, \nu}| \geq t\right) \geq e^{-\epsilon \frac{n q_n}{2}} \frac{M - t - a}{b - a}.$$

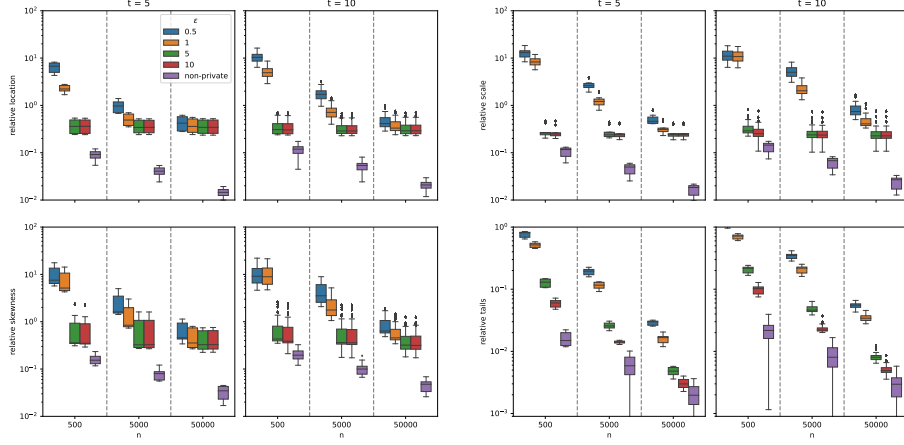


Figure 9: Average pair-wise relative boxplot distances (y-axis) between multiple private boxplots in terms of relative location, scale, skewness and outliers, under varying conditions of $\epsilon \in \{0.5, 1, 5, 10\}$ (color), $n \in \{500, 5000, 50000\}$ (x-axis); using DPBoxplot quantile estimation and $t \in \{5, 10\}$ (columns). Legend non-private is the relative similitude between the non-private boxplots.

Proof. We have that

$$\Pr\left(|\tilde{\xi}_{q_n} - \xi_{q_n, \nu}| \geq t\right) \geq \Pr\left(\tilde{\xi}_{q_n} \leq M - t\right) \geq \frac{\int_a^{M-t} e^{-\epsilon \frac{n|F_{\hat{\nu}}(x) - q_n|}{2}} dx}{\int_a^b e^{-\frac{n|F_{\hat{\nu}}(x) - q_n|}{2\epsilon}} dx} \geq e^{-\epsilon \frac{nq_n}{2}} \frac{M - t - a}{b - a}.$$

□

In this case, if $q_n = n^{-k}$, then the sample complexity is then at least $O((\log(1/\gamma) \cdot \frac{M-t-a}{b-a})/\epsilon)^{1/(1-k)}$.

Lemma 9. For all $n \geq 1$, $a, c \in \mathbb{R}$, we have that $n \geq a \log n + c$ if $n \geq 2(a \log a + c) \vee a$.

Proof. First, note that $h(n) = n - a \log n - c$ is increasing for $n \geq a$. Now, for $n \geq a$ we can use the fact that $x - \log x \geq x/2$ for $x \geq 1$ to get $h(n) \geq 0$ whenever $n \geq 2(a \log a + c)$. □

Let \mathcal{B} denote the space of Borel functions from \mathbb{R}^d to $[0, 1]$. For a family of functions, $\mathcal{F} \subseteq \mathcal{B}$, define a pseudometric on $\mathcal{M}_1(\mathbb{R}^d)$, $d_{\mathcal{F}}(\mu, \nu) = \sup_{g \in \mathcal{F}} |\int g d(\mu - \nu)|$, where $\mu, \nu \in \mathcal{M}_1(\mathbb{R}^d)$.

Definition 2 (Ramsay et al. (2024)). We say that $\phi(x, \nu)$ is (K, \mathcal{F}) -regular if there exists a class of functions $\mathcal{F} \subseteq \mathcal{B}$ such that $\phi(x, \cdot)$ is K -Lipschitz with respect to the \mathcal{F} -pseudometric uniformly in x , i.e., for all $\mu, \nu \in \mathcal{M}_1(\mathbb{R}^d)$

$$\sup_x |\phi(x, \mu) - \phi(x, \nu)| \leq K d_{\mathcal{F}}(\mu, \nu).$$

D Broader impacts

Our proposed methodology inherits the extensive implications, both beneficial and detrimental, of differential privacy. Differential privacy significantly enhances data confidentiality by introducing noise into datasets, which complicates the ability to link specific data points to individual identities. This greatly enhances the privacy awarded to individuals whose information is contained in such datasets. However, this method is not without its drawbacks. The primary challenge lies in the trade-off between privacy protection and data accuracy. The introduction of noise, while safeguarding privacy, may distort the data, potentially yielding inaccurate insights or conclusions. Such inaccuracies are especially problematic in contexts requiring high precision, such as policy development or clinical research, where exact data is crucial.